Research Paper

Numerical Comparison of Two Runners for Gravitational Vortex Turbine

Alejandro RUIZ SÁNCHEZ[1)]*, Angie GUEVARA MUÑOZ[1)]
Jorge Andrés SIERRA DEL RIO[2)], Jose Alejandro POSADA MONTOYA[2)]

[1)] *Department of Mechatronics Engineering, MATyER*
Instituto Tecnológico Metropolitano Medellín
Colombia
*Corresponding Author e-mail: alejandroruiz190787@correo.itm.edu.co

[2)] *Department of Mechanical Engineering, GIIAM*
Institución Universitaria Pascual Bravo Medellín
Colombia

The main purpose of this study is to compare numerically the torque generated by two runners for a gravitational vortex turbine. One of the runners was an H-Darrieus turbine with the rotational flow into the chamber that helped to decrease its negative torque. The other runner was a standard (straight blade) turbine, which determined the performance in both cases. The study was conducted in ANSYS®CFX, where the model was configured at constant operating conditions in both cases. The standard runner performance was higher (75%) than that of the H-Darrieus runner. The highest torque for the standard and the H-Darrieus runners was 0.76 and 0.16 N · m, respectively. The standard runner had a larger fluid contact area than the H-Darrieus runner, which extracted more energy.

Key words: vortex; runner; H-Darrieus; geometry; performance.

1. INTRODUCTION

Renewable energies are increasingly important to satisfy global energy demand. Since the beginning of the last decade, they have experienced an annual growth of around 8–9% [1], and it is expected that by 2023 they will supply at least 30% of world electricity demand, according to the International Energy Agency. Hydroelectric power is the largest renewable energy source in the world. It supplies around 16% of the world consumption [1] and only Latin America and the Caribbean have 20% of the world's water potential. However, about 30 million people do not have electricity service [2]. They are in geographically isolated or difficult access areas, which prevents coverage by the national electricity

systems. Due to this situation, some communities have opted for using renewable energies [3], such as small hydroelectric power plants (PCHs), which minimize negative impacts on the environment. They have low emissions of greenhouse gases (GHG) and do not require large structures for their implementation compared to large hydroelectric [4]. Among them, there are the gravitational vortex turbine (GVT) power plants (PCHs), which are open hydraulic systems that operate with the natural current of the river. This is economical and does not require considerable civil works for their construction [5]. GVT is mainly comprised of a chamber that has a water inlet channel that stabilizes the fluid and leads it to the chamber. Due to chamber geometry and tangential and axial velocity, a pre-rotation of the water is created, which is affected by the force of gravity and the Coriolis force [6], creating an induced water vortex. This turbulent flow is harnessed by a runner that transmits the water kinetic energy to an energy transformer [7]. Figure 1 graphically represents the GVT parts.
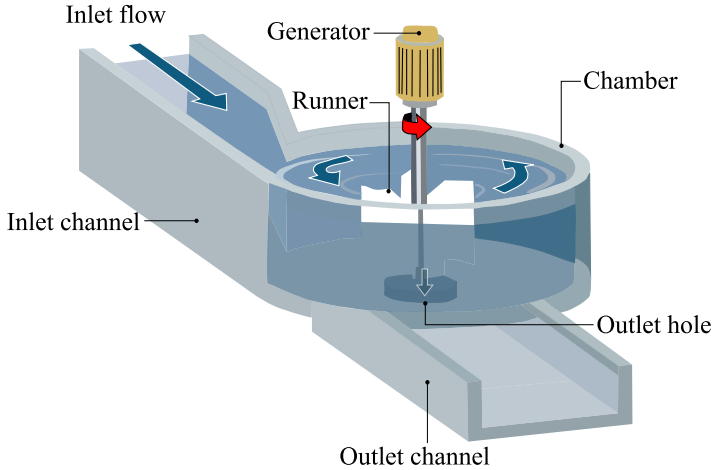

Fig. 1. GVT parts.

To summarize the literature review on GVTs, Table 1 presents the main studied aspects related to GVTs according to the authors' knowledge. The table shows that the main studied parameters focus on chamber geometry (8 studies), compared to few studies carried out on the runner (4 studies) of a GVT.

In order to evaluate the performance of a new runner geometry, an H-Darrieus turbine was selected. One of the main areas of interest in the mentioned above turbine is the negative torque of the incoming blade [23]. This phenomenon occurs when the flow direction affects the incoming blade runner. In the case of GVT, the flow is rotational inside the chamber, and for this reason, it was assumed that the negative torque decreases considerably if an H-Darrieus turbine

Table 1. Literature review summary.

Main parameter	Kind of study	Major findings	Reference
Water inlet height	CFD and experimental	Result differences between 0% and 7%	[8]
Turbulence model	Analytical, CFD and experimental	Baseline Reynolds stress model	[9]
Chamber geometry	CFD and experimental	Cylindrical	[10]
		Conical	[11]
		Concave and convex	[12]
Chamber diameter Angle of the reduction zone Width of the inlet channel Angle of the cone Channel height	CFD	0.8 m 70° 0.125 D 23° 0.2 D	[13]
Outlet diameter for a conical chamber	CFD	0.3 D	[14]
Ratio between the chamber diameter and the outlet diameter (D/d) Inlet channel slope angle	CFD	2.5 60°	[15]
Outlet diameter	CFD and experimental	0.14 $D - 0.18$ D	[16]
Number of blades in the runner (according to geometry)	CFD and experimental	12	[17]
Thickness of runner blades (according to geometry)	CFD and experimental	Blade thickness	[18]
Blade profile in the runner	CFD	Curved profile	[19, 20]
Multi-stage runner	Experimental	Multi-stage runner	[21, 22]
Economic evaluation	Experimental	Economic feasibility	[5]

is implemented as a GVT runner, increasing the performance. The purpose of this study is to numerically evaluate and compare the performance of GVT with two different runners (H-Darrieus and standard).

2. Methodology

2.1. Governing equations

There is no a standard model to characterize the vortex and an equation for relationship between geometrical parameters and power generation. Some authors do not provide enough information about the model used, so there is no way to standardize the equation or have a reference for future studies.

Table 2 shows different mathematical correlations in the literature to characterize the vortex and governing equation. In fact, inside the GVT chamber, both fluids (water and air) share the same physical properties, i.e., velocity fields and turbulence. The governing equations for the unsteady, viscous and vortex formation's turbulent flow are the continuity and Navier-Stokes equations described in Eqs (2.12) and (2.13), respectively. Those equations (continuity and Navier-Stokes) were developed by software ANSYS® in its 2019-R3 version.

Table 2. Mathematical models developed to characterize the vortex generated inside the GVT and governing equation.

Author	Tangential velocity equation	Comments	Number
Mathematical models to characterize the vortex formed			
Mulligan et al. [9]	$v_\theta(r) \propto 1/r$	–	(2.1)
Einstein, Li [24]	$v_\theta(r) = \dfrac{\Gamma}{2\pi r}$	–	(2.2)
Vatistas et al. [25]	$v_\theta(r) = \dfrac{\Gamma}{2\pi}\left(\dfrac{r}{(r_c^4 + r^4)^{1/2}}\right)$	when $0 \leq r \leq \infty$	(2.3)
Rosenhed [26]	$v_\theta(r) = \dfrac{\Gamma}{2\pi}\left(\dfrac{r}{(r_c^2 + r^2)}\right)$	–	(2.4)
Hite, Mih [27]	$v_\theta(r) = \dfrac{\Gamma}{2\pi}\left(\dfrac{2r}{(r_c^2 + 2r^2)}\right)$	–	(2.5)
Odgaard [28]	$V_\theta(r) = \dfrac{\Gamma}{2\pi}\left[1 - \exp\left(-\dfrac{1}{4}\dfrac{v_z}{Hv}r^2\right)\right]$	–	(2.6)
Rankine [29]	$v_\theta(r) = \omega r = \dfrac{\Gamma}{2\pi}\dfrac{r}{r_c^2}$	when $r < r_c$	(2.7)
	$v_\theta(r) = \dfrac{\Gamma}{2\pi r} = \omega\dfrac{r_c^2}{r}$	when $r > r_c$	(2.8)
Burgers [30]	$v_\theta(r) = \dfrac{EC}{2\pi r}\left(e^{\frac{-\mathrm{E}r^2}{2\pi}}\right)$	–	(2.9)
Rahman et al. [31]	$v_\theta(r) = \dfrac{(\Gamma_\infty)(r_c)}{\sqrt{[8\,(r_c^2)\,(g)\,(\pi^2)\,(H-h) + \Gamma_\infty^2]}}$	–	(2.10)
Marian et al. [32]	$v_\theta(r) = \dfrac{\Gamma d\sqrt{2(g)(H+h)}}{2(\pi)(r)}$	–	(2.11)
Governing system equations			
Continuity	$\dfrac{\partial v_r}{\partial r} + \dfrac{\partial v_z}{\partial Z} + \dfrac{v_r}{r} = 0$	–	(2.12)
Navier-Stokes	$\dfrac{\partial \mathbf{v}}{\partial t} + \mathbf{v}\cdot(\nabla\mathbf{v}) = \dfrac{-1}{\rho}\nabla p + \nu\nabla^2\mathbf{v} + \mathbf{g}$	–	(2.13)

In Table 2, the following notations have been adopted: v_θ, v_r, and v_z are tangential, radial, and axial velocity, respectively, Γ is circulation, r is water radius, r_c is the air core radius, ν is kinetic viscosity, C and E are constants, g is gravity acceleration, H is vortex height, h is point height, and

$$(2.14) \qquad \Gamma = \oint_L \mathbf{v} \cdot d\mathbf{l},$$

where $\mathbf{v}$ is the velocity field and L is the vertical axis at the surface. However, Stoke's theorem expresses the previous equation with a rotational velocity field:

$$(2.15) \qquad \Gamma = \iint_A (\nabla \times \mathbf{v}) \cdot d\mathbf{A},$$

where A is the surface area, and the rotational velocity field $(\nabla \times \mathbf{v})$ is equal to vector field vorticity $(\mathbf{\Omega})$, Eq. (2.16) is expressed as:

$$(2.16) \qquad \Gamma = \iint_A \mathbf{\Omega} \cdot d\mathbf{A}.$$

For the Navier-Stokes equation, $\mathbf{v}$ represents the velocity vector and it is defined in Eq. (2.17), and ∇ reduces the partial derivation in each component (x, y, z) and it is explained in Eq. (2.18)

$$(2.17) \qquad \mathbf{v}_k = (u, y, w),$$

$$(2.18) \qquad \nabla = \frac{\partial}{\partial x}, \frac{\partial}{\partial y}, \frac{\partial}{\partial z}.$$

To exemplify the variables in Table 2, Fig. 2 shows the physical behavior of a water particle (wp) inside the GVT chamber. Front (left side) and top (right) views are shown.
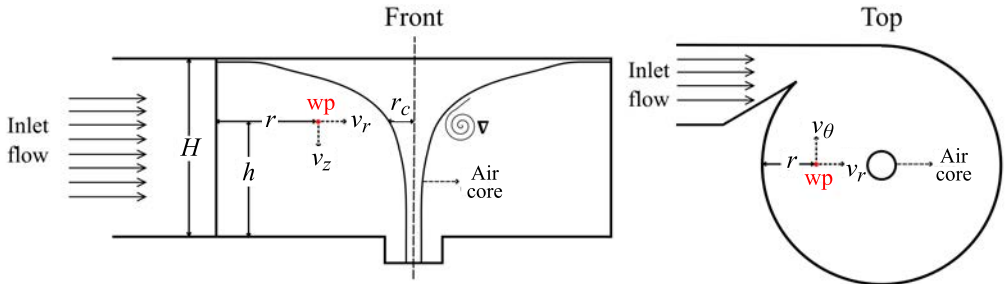

FIG. 2. Velocity profiles and variables for wp inside the GVT chamber.

2.2. *Volume control*

Among the different geometries reported in the state of art research are the cylindrical [10], concave, convex [12], and conical chambers [11]. The latter ones show an increment in vortex tangential velocity and power generation [11]. For this reason, a conical chamber was selected.

Figure 3a shows a top view of a GVT domain and its respective design parameters. Figure 3b shows a plane view section (A-A) and exemplifies the domains established for the present study. The static domain corresponds to the GVT chamber, and the rotating domain corresponds to the runners that were studied. The same dimensions were used for both runners. The symbols (parameters) mentioned in Fig. 3 will be explained later in Table 3.
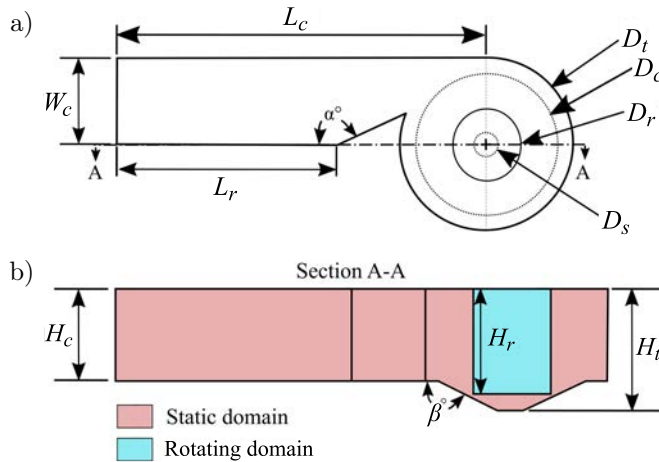

FIG. 3. Top and cut view from GVT domain studies:
a) GVT top view, b) GVT and runner cut view.

From left to right, Table 3 shows the parameters considered (Fig. 3), their symbols and values assigned for the chamber design. It should be noted that the conical section is observed from the bottom of the chamber. Furthermore, the chamber with a D_s/D_t ratio equal to 14% [16] was considered. Similarly, the parameters, symbols and values of the rotating domain (runner) are shown in Table 4. It should also be noted that the values were taken according to the performance presented in previous studies.

Once the design was modeled, the discretization was carried out in the ICEM CFD module of ANSYS®. Hexahedral elements were used to represent the internal volume of the chamber and runner assembly. Figure 4a shows the chamber discretization, identifying the inflation in the chamber walls and considering the viscous friction that can cause hydraulic losses. Figure 4b shows a top view of

Table 3. Design parameters for the static domain.

Parameter	Symbol	Value
Channel height	H_c	0.30 m
Channel width	W_c	0.35 m
Channel length	L_c	1.5 m
Notch length	L_r	0.9 m
Notch angle	α	155°
Chamber height	H_t	0.4 m
Chamber diameter	D_t	0.7 m
Conical angle	β	67°
Outlet hole diameter	D_s	0.098 m
Rotating domain diameter	D_r	0.25 m
Rotating domain height	H_r	0.35 m

Table 4. Design parameters for the rotational domain.

Parameter	H-Darrieus [23]	Standard [19]
Diameter	0.2 m	0.2 m
Height	0.13 m	0.13 m
Aspect ratio	0.68	0.68
Blades number	3	4
Profile	NACA 2408	N/A
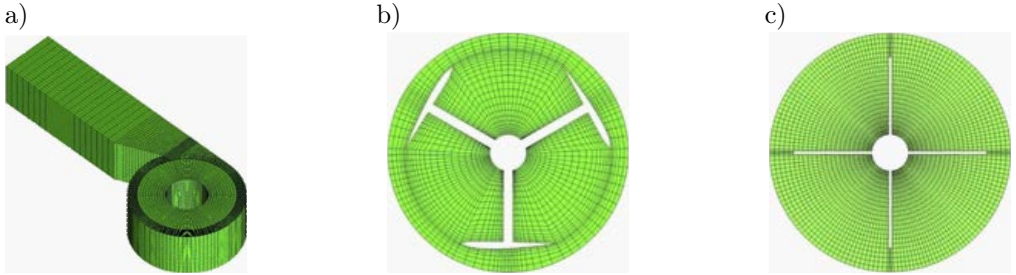
FIG. 4. Static and rotating domains meshes: a) static domain (chamber), b) rotating domain H-Darrieus runner, c) rotating domain standard runner.

the rotating domain of the H-Darrieus runner, where the inflation is close to the blade's wall. Figure 4c represents the top view of the standard runner. As previously mentioned, the blades are straight. In addition, they produce the same inflation close to each blade's wall. The meshes metrics are detailed in Table 5, and they are in the acceptable ranges [33].

Table 5. Mesh metrics for static and rotating domains.

Domain	Number of elements	Min. determinant $3 \times 3 \times 3$	Max. aspect ratio	Min. quality
H-Darrieus	259.932	0.440	26	0.440
Standard	311.045	0.768	8.080	0.768
Chamber	30.305	0.459	7.050	0.381

The boundary conditions associated with the volume control were configured to biphasic fluid (air and water). Both fluids are at a temperature of 25°C, a relative pressure of 0 Pa and a volume fraction with zero gradients for the opening and outlet. The inlet was configured as normal water inlet to surface with a constant velocity of 0.2 m/s. In addition, the slip-free torque condition was set as a representation of the GVT surfaces in wall configuration. For the rotating domain, an angular velocity was established from 25 to 100 rpm with increments of 25 rpm. A transient runner-stator interface was configured in each domain in order to create a connection between the mesh of both domains and was declared fluid-fluid. This guarantees that the calculated variable (torque) corresponds to a system that varies over time. Figure 5 represents the boundary conditions established for the static and rotating domains.
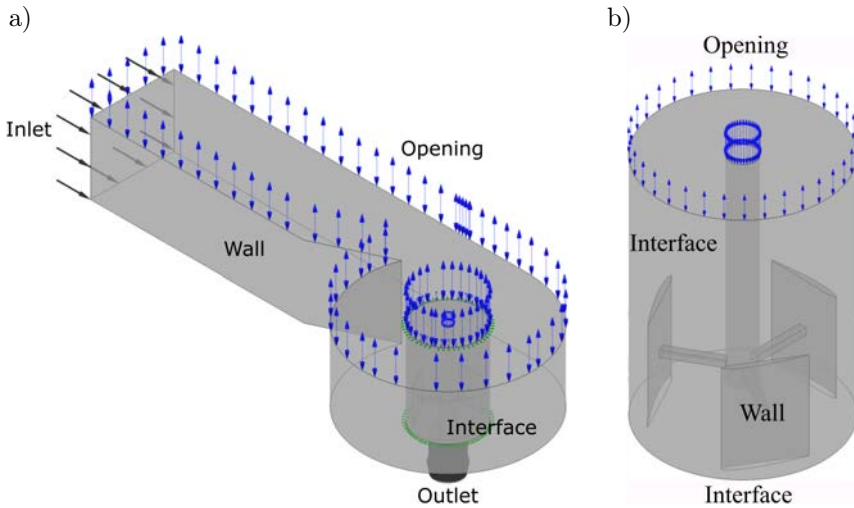

FIG. 5. Boundary conditions for the static and rotating domains: a) boundary condition for the static domain, b) boundary condition for the rotating domain.

The simulation was carried out in the ANSYS® CFX module and configured in a transient state with a convergence criterion of 1E-4 [34–36]. High resolution was used for the advection scheme and the backward Euler's second-order

equation was configured to reduce numerical uncertainty [35]. The total simulation time was 15 s (to visualize the start-up and stabilization of the system) with an adaptive time-step (Δt) between 0.001 s and 0.0001 s. The higher Δt was calculated, guaranteeing a Courant number less than 1 [36]. The baseline Reynolds stress model turbulence model was selected, offering greater precision in the rotating system, such as the flow of a vortex [9].

3. Results and discussion

Figure 6 represents the mesh independence study carried out for each case study at a rotational velocity of 25 rpm for the rotating domain. The meshes selected for the rotating domain in each case were approximately 259E3 and 311E3 elements for the H-Darrieus and standard runner, respectively. For the static domain, a mesh of 30E3 elements was simulated. The meshes were selected because they represent a difference in results lower than 5% compared to the previous mesh. The mesh independence study guarantees that results are not affected by the number of elements [34–38].
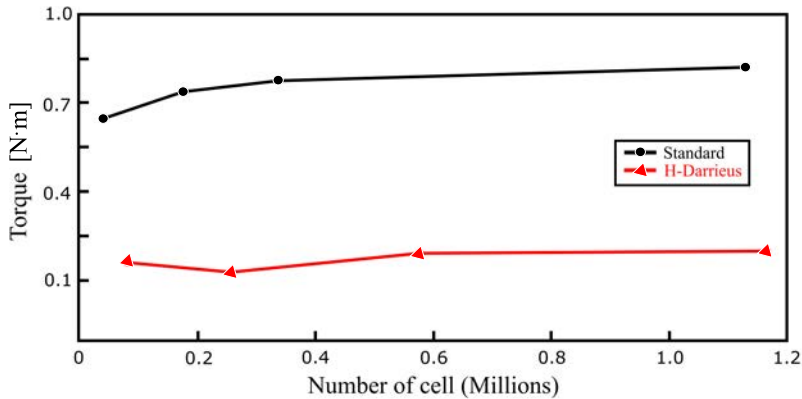

Fig. 6. Mesh independence for both cases.

Figure 7 shows the variation of the generated torque for each configured runner's geometry against the angular velocity, from 25 rpm to 100 rpm. In this figure, the torque for both cases decreases at higher revolutions and the great difference in the power between the H-Darrieus runner (red) and the standard runner (black) is generated. The point to measure the variable was the runner shaft. Both cases presented the highest torque at a velocity of 25 rpm and decreased as the velocity increased. The highest torque values were 0.76 N·m and 0.16 N·m for the standard runner and the H-Darrieus runner, respectively. This shows that the standard runner has a better performance (75%) than the H-Darrieus runner.
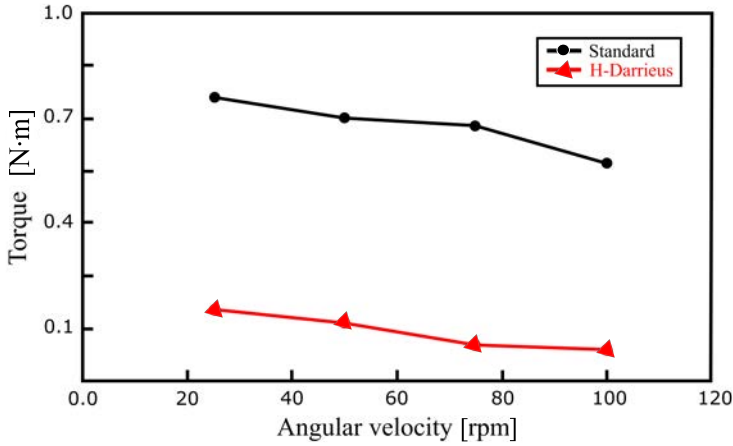
Fig. 7. Torque variation against angular velocity for both cases.

The standard runner blades have a greater contact area than the H-Darrieus runner blades. This helps to interact with more water, and therefore more energy can be extracted. It should be noted that both runners are intrusive and deform the vortex considerably. The H-Darrieus runner works by lift force [23]. However, in this study, greater drag force is present due to fluid behavior (rotating around the chamber).

Figure 8 shows an isometric and front view of water streamlines and fluid vectors within the chamber for the H-Darrieus (Fig. 8a) and standard runner (Fig. 8b). It is possible to observe how the flow enters and stabilizes in the channel. In addition, the fluid increases its velocity in the reduction area before to the chamber. The streamlines show how the water velocity increases as it descends through the chamber and moves rapidly to the bottom of the chamber until it interacts with the runner. However, the front view of Fig. 8b shows that the standard runner is more intrusive in the chamber than the H-Darrieus runner. As mentioned before, the more intrusive the runner, the more fluid it interacts with, allowing to extract more energy. However, it should be considered that the greater the radius of the runner, the more it will interact with a water volume fraction of lower velocity compared to the fluid near the vortex.

Figure 9 shows the water pressure contours in the standard and H-Darrieus blade runners. In both cases, it is observed that the highest pressure point is at the bottom of the runners. This is because the fluid increases its velocity as it descends through the chamber and approaches the center of the vortex [11]. However, in the standard runner (left) it is observed that there is a greater contact area for fluid, which provides a larger cross-sectional area for the pressure, where the highest pressure value is 2.43 kPa. Unlike the H-Darrieus runner
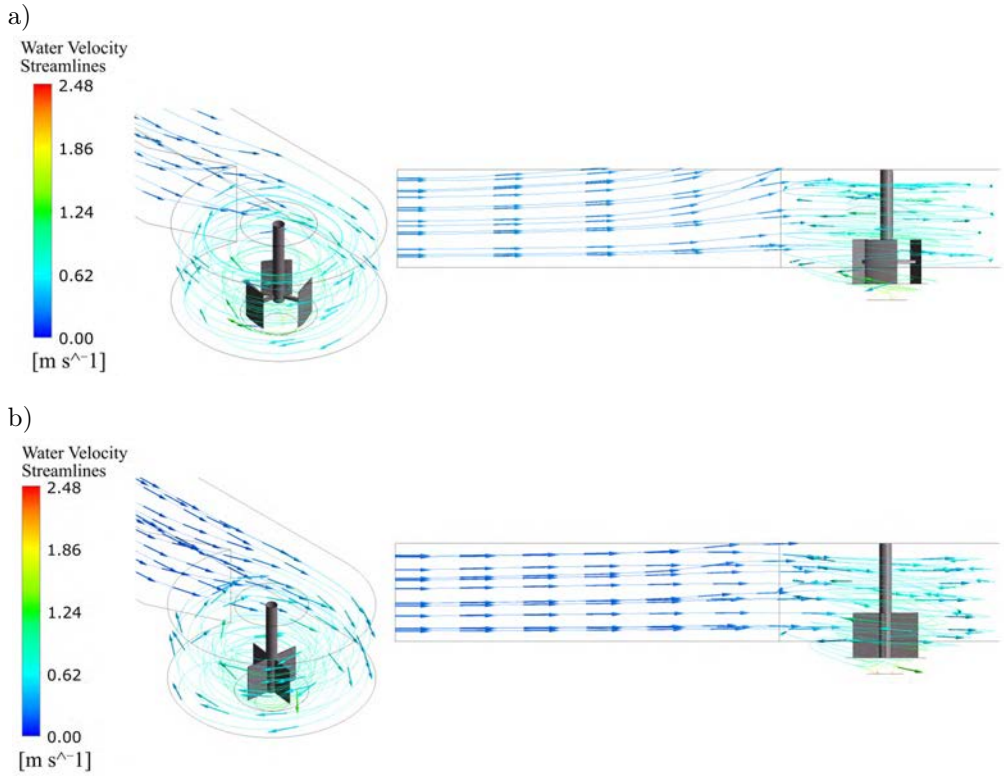
a)

b)

FIG. 8. Isometric and frontal view for water velocity streamlines inside the chamber for both cases: a) water velocity streamlines for the H-Darrieus runner, b) water velocity streamlines for the standard runner.
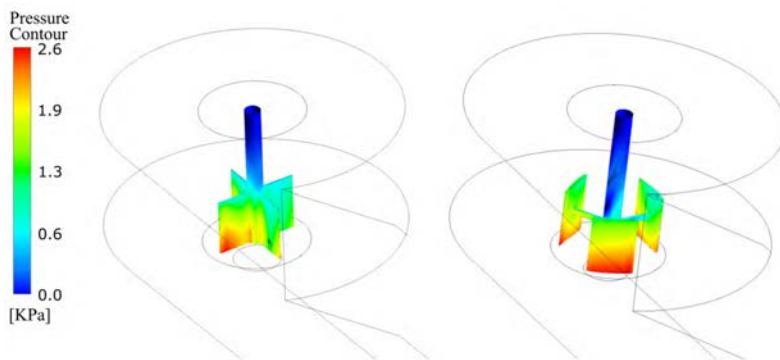

FIG. 9. Water pressure contour in blades runners.

(right), where the highest pressure value of 2.35 kPa is observed when the pressure is exerted on the blade tip, where there is a smaller contact area for fluid.

The aim of this article was to numerically compare a runner geometry that had not been studied. Thus, thanks to the present study, it can be determined that the fluid contact area with the blade runner is a parameter that considerably influences the turbine performance. Despite the difference being less than 1% at the highest pressure point, this means a difference above 75% in performance due to the cross-sectional area.

4. Conclusion

A numerical comparison of torque generated between a standard (straight blade) and an H-Darrieus runner was performed for a gravitational vortex turbine. The study was carried out in the ANSYS® 2019-R3 software in its ICEM-CFD and CFX modules. The performance of each runner was determined, and it was be concluded that:

- The runner design considerably affects the performance of the GVT; parameters such as the type and number of blades greatly affect the performance of the turbine.

- The standard runner showed a better performance compared to the H-Darrieus runner. The blade contact area helped to extract more energy from the fluid. Consequently, it allowed a higher performance in GVT. However, it must be considered that the larger the runner, the more it will interact with water volume fractions with lower velocity.

- The H-Darrieus runner increases its performance with the lifting principle. Nevertheless, due to the rotation of the fluid in the chamber, a greater drag force is present. However, it was possible to show that the negative torque in the inlet blade was lower and it can serve to increase the performance of the H-Darrieus as a turbine.

- Thanks to its easy fabrication and low maintenance requirements, the GVT is a good alternative to supply electrical energy to non-interconnected areas and with changes in its chamber or runner geometry, its performance can be improved.

5. Future works

According to the literature review and the present study, the runner geometry considerably affects the turbine performance. For future works, different geometries for the runner as well as the Savonius turbine can be studied because the main force of this turbine's runner is the drag force. Furthermore, in the future, the present numerical results should be confirmed with experimental results.

References

1. IRENA – International Renewable Energy Agency, *Renewable capacity highlights*, No. March, p. 2, 2018.

2. Millán J., *Water and energy* [in Spanish: *Agua y Energía*], Caracas, Venezuela, Aug. 2015.

3. Dyner I., Alvarez C., Cherni J., Energy contribution to sustainable rural livelihoods in developing countries: a system dynamics approach, [in:] *Proceedings of 23rd International Conference of the System Dynamics Society*, July 17–21, 2005, Boston, USA, 2005.

4. Perius M.R., Carregaro J.B., Small hydroelectric plants as a way of reducing environmental impacts and energy crises, *Essays and Science Biological, Agricultural and Health Sciences* [in Portuguese: Pequenas centrais hidrelétricas como forma de redução de impactos ambientais e crises energéticas, *Ensaios e Cięncia Cięncias Biológicas, Agrárias e da Saúde*], **16**(2): 135–150, 2012, doi: 10.17921/1415-6938.2012v16n2p%25p.

5. Alzamora Guzmán V.J., Glasscock J.A., Whitehouse F., Design and construction of an off-grid gravitational vortex hydropower plant: A case study in rural Peru, *Sustainable Energy Technologies and Assessments*, **35**: 131–138, 2019, doi: 10.1016/ j.seta.2019.06.004.

6. Li H-F., Chen H-X., Ma Z., Zhou Y., Formation and influencing factors of free surface vortex in a barrel with a central orifice at bottom, *Journal of Hydrodynamics*, **21**(2): 238–244, 2009, doi: 10.1016/S1001-6058(08)60141-9.

7. Timilsina A.B., Mulligan S., Bajracharya T.R., Water vortex hydropower technology: a state-of-the-art review of developmental trends, *Clean Technologies and Environmental Policy*, **20**(8): 1737–1760, 2018, doi: 10.1007/s10098-018-1589-0.

8. Shabara H.M., Yaakob O.B., Ahmed Y.M., Elbatran A. H., Faddir M.S.M., CFD validation for efficient gravitational vortex pool system, *Jurnal Teknologi.*, **74**(5): 97–100, 2015, doi: 10.11113/jt.v74.4648.

9. Mulligan S., Casserly J., Sherlock R., Experimental and numerical modelling of free-surface turbulent flows in full air-core water vortices, [in:] Gourbesville P., Cunge J., Caignaert G. [Eds], *Advances in Hydroinformatic*, pp. 549–569, Springer Singapore, Singapore, 2014, doi: 10.1007/978-981-287-615-7_37.

10. Wanchat S., Suntivarakorn R., Preliminary design of a vortex pool for electrical generation, *Advanced Science Letters*, **13**(1): 173–177, 2012, doi: 10.1166/asl.2012.3855.

11. Dhakal S. *et al.*, Comparison of cylindrical and conical basins with optimum position of runner: Gravitational water vortex power plant, *Renewable and Sustainable Energy Reviews*, **48**: 662–669, 2015, doi: 10.1016/j.rser.2015.04.030.

12. RUIZ SÁNCHEZ A., SIERRA DEL RIO J.A., GUEVARA MUŃOZ A. J., POSADA MON-TOYA J.A., Numerical and experimental evaluation of concave and convex designs for gravitational water vortex turbine, *Journal of Advanced Research in Fluid Mechanics and Thermal Sciences*, **64**(1): 160–172, 2019.

13. DHAKAL S., TIMILSINA A.B., DHAKAL R., FUYAL D., BAJRACHARYA T.R., PAN-DIT H.P., Effect of dominant parameters for conical basin: gravitational water vortex power plant, [in:] *International Conference on Technolog and Innovation Management & IOE*, **1**: 380–386, 2014.

14. SREERAG S.R., RAVEENDRAN C.K., JINSHAH B.S., Effect of outlet diameter on the performance of gravitational vortex turbine with conical basin, *International Journal of Scientific & Engineering Research*, **7**(4): 457–463, 2016.

15. REHMAN W., IJAZ M., MUNIR A., Designing of micro gravitational vortex turbine's vortex pool, *Proceedings of the ASME 2017 Power Conference*, Vol. 2, Charlotte, North Carolina, USA, June 26–30, 2017, doi: 10.1115/POWER-ICOPE2017-3186.

16. WANCHAT S., SUNTIVARAKORN R., WANCHAT S., TONMIT K., KAYANYIEM P., A para-metric study of gravitational vortex power plant, *Advanced Materials Research.*, **805–806**: 811–817, 2013, doi: 10.4028/www.scientific.net/AMR.805-806.811.

17. DHAKAL S., NAKARMI S., PUN P., THAPA A.B., BAJRACHARYA T.R., Development and testing of runner and conical basin for gravitational water vortex power plant, *Journal of the Institute of Engineering*, **10**(1): 140–148, 2014, doi: 10.3126/jie.v10i1.10895.

18. WICHIAN P., SUNTIVARAKORN R., The effects of turbine baffle plates on the efficiency of water free vortex turbines, [in:] *3rd International Conference on Power and Energy System Engineering*, 2016, pp. 8–12.

19. DHAKAL R. *et al.*, Computational and exerimental investigation of runner for gravitational water vortex power plant, *2017 IEEE 6th International Conference on Renewable Energy Research and Applications (ICRERA)*, San Diego, CA, 2017, Vol. 5, pp. 365–373, 2017, doi: 10.1109/ICRERA.2017.8191087.

20. SALEEM A.S. *et al.*, Parametric study of single-stage gravitational water vortex turbine with cylindrical basin, *Energy*, **200**: 117464, 2020, doi: 10.1016/j.energy.2020.117464.

21. ULLAH R., CHEEMA T.A., SALEEM A.S., AHMAD S. M., CHATTHA J.A., PARK C.W., Performance analysis of multi-stage gravitational water vortex turbine, *Energy Conversion and Management*, **198**: 111788, 2019, doi: 10.1016/j.enconman.2019.111788.

22. ULLAH R., CHEEMA T.A., SALEEM A.S., AHMAD S. M., CHATTHA J.A., PARK C.W., Preliminary experimental study on multi-stage gravitational water vortex turbine in a con-ical basin, *Renewable Energy*, **145**: 2516–2529, 2020, doi: 10.1016/j.renene.2019.07.128.

23. PATEL V., ELDHO T.I., PRABHU S.V., Performance enhancement of a Darrieus hydroki-netic turbine with the blocking of a specific flow region for optimum use of hydropower, *Renewable Energy*, **135**: 1144–1156, 2019, doi: 10.1016/j.renene.2018.12.074.

24. EINSTEIN H.A., LI H., Steady vortex flow in a real fluid, *Proceding of Heat Transfer and Fluid Mechanics Institute, Stanford University*, pp. 33–43, 1951.

25. VATISTAS G.H., LIN S., KWOK C.K., Theoretical and experimental studies on vortex chamber flows, *AIAA Journal*, **24**(4): 635–642, 1986, doi: 10.2514/3.9319.

26. ROSENHEAD L., The spread of vorticity in the wake behind a cylinder, *Proceedings of the Royal Society of London. Series A. Mathematical, Physical and Engineering Sciences*, **127**(806): 590–612, 1930, doi: 10.1098/rspa.1930.0078.

27. HITE JR, J.E., MIH W.C., Velocity of air-core vortices at hydraulic intakes, *Journal of Hydraulic Engineering*, **120**(3): 284–297, 1994.

28. ODGAARD A.J., Free-surface air core vortex, *Journal of Hydraulic Engineering*, **112**(7): 610–620, 1986, doi: 10.1061/(ASCE)0733-9429(1986)112:7(610).

29. RANKINE W.J.M., *A Manual of Applied Mechanics*, London: Charles Griffin and Co., 1858.

30. BURGERS J.M., A mathematical model illustrating the theory of turbulence, *Advances in Applied Mechanics*, **1**(C): 171–199, 1948, doi: 10.1016/S0065-2156(08)70100-5.

31. RAHMAN M., HONG T.J., TANG R., SUNG L.L., TAMIRI F.B.M., Experimental study the effects of water pressure and turbine blade lengths & numbers on the model free vortex power generation system, *International Journal of Current Trends in Engineering & Research (IJCTER)*, **2**(9): 13–17, 2016.

32. MARIAN M.G., SAJIN T., AZZOUZ A., Study of micro hydropower plant operating in gravitational vortex flow mode, *Applied Mechanics and Materials*, **371**: 601–605, 2013, doi: 10.4028/www.scientific.net/AMM.371.601.

33. Ansys Inc., *User Manual Ansys ICEM CFD 12.1*, vol. 0844682, no. November, pp. 724–746, 2009.

34. CEBALLOS CASTAŃEDA Y.C., VALENCIA C.M., ZULUAGA H.D., DEL RIO J., GARCIA V.S., Influence of the number of blades in the power generated by a Michell Banki Turbine, *International Journal of Renewable Energy Research-IJRER*, **7**(4): 1989–1997, 2017.

35. ROACHE P.J., GHIA K.N., WHITE F.M., Editorial policy statement on the control of numerical accuracy, *Journal of Fluids Engineering*, **108**(1): 2, 1986, doi: 10.1115/1.3242537.

36. ANSYS, Courant number, [in:] *ANSYS Help*, 2019.

37. BELTRAN-URANGO D., HERRERA-DÍAZ J.L., POSADA-MONTOYA J.A., CASTAŃEDA L., SIERRA-DEL RIO J.A., Generation of Electric Power Through Gravitational Vortices [in Spanish: Generación de Energía Eléctrica Mediante Vórtices Gravitacionales], Memorias EXPO Tecnologias 2016, Medellin, Antioquia, pp. 90–107, 2016.